Chaotic dynamics of a magnetic nanoparticle

J. Bragard,[1] H. Pleiner,[2] O. J. Suarez,[3] P. Vargas,[3] J. A. C. Gallas,[4,5] and D. Laroze[2,6,*]

[1]*Departamento de Física y Matemática Aplicada, Universidad de Navarra, E-31080 Pamplona, Spain*

[2]*Max Planck Institute for Polymer Research, D-55021 Mainz, Germany*

[3]*Departamento de Física, Universidad Técnica Federico Santa María, Casilla 110-V, Valparaíso, Chile*

[4]*Institute for Multiscale Simulations, Friedrich-Alexander Universität, D-91052 Erlangen, Germany*

[5]*Departamento de Física, Universidade Federal da Paraíba, BR-58051-970 João Pessoa, Brazil*

[6]*Instituto de Alta Investigación, Universidad de Tarapacá, Casilla 7D, Arica, Chile*

(Received 9 March 2011; revised manuscript received 9 June 2011; published 21 September 2011)

We study the deterministic spin dynamics of an anisotropic magnetic particle in the presence of a magnetic field with a constant longitudinal and a time-dependent transverse component using the Landau-Lifshitz-Gilbert equation. We characterize the dynamical behavior of the system through calculation of the Lyapunov exponents, Poincaré sections, bifurcation diagrams, and Fourier power spectra. In particular we explore the positivity of the largest Lyapunov exponent as a function of the magnitude and frequency of the applied magnetic field and its direction with respect to the main anisotropy axis of the magnetic particle. We find that the system presents multiple transitions between regular and chaotic behaviors. We show that the dynamical phases display a very complicated structure of intricately intermingled chaotic and regular phases.

DOI: 10.1103/PhysRevE.84.037202 PACS number(s): 05.45.Pq, 75.10.Hk, 75.40.Mg

The world of nanometric scale is becoming increasingly accessible due to the remarkable development of experimental techniques. The technological applications of nanostructures can be found in many different areas such as biomedicine or high-precision instrumentation. In material science, one significant application of magnetic particles and clusters is in the area of recording media [1] and so the magnetization reversal is one of the fundamental features of data storage. Therefore, a detailed study of a simple magnetic systems is really important and will be presented here.

Nonlinear time-dependent problems in magnetism have already been studied in numerous cases where the standard approaches to modeling the classical magnetic dynamics use the Landau-Lifshitz or Landau-Lifshitz-Gilbert (LLG) equation; recent accounts of developments can be found in Refs. [2,3]. These models have been used in both discrete [3–7] and continuous magnetic systems [3,8,9]. Several experiments showing chaotic behavior in magnetic systems have been reported [10–13]. Typical magnetic samples are yttrium iron garnet spheres [10]. It is worth mentioning that by using ferromagnetic resonance technique, different routes to chaos have been found such as period-doubling cascades, quasiperiodic dynamics, and intermittent dynamics. Hence a theoretical description including phase diagrams of the chaotic regions is needed and can motivate further experiments in this area.

Here we report the computation of complete phase diagrams for a chaotic nanoparticle governed by the LLG equation. Complete phase diagrams, namely, diagrams recording all physically stable phases, both periodic and chaotic, are relatively hard to obtain because they imply computationally intensive calculations, particularly for models described by flows, i.e., by continuous systems of ordinary differential equations. Recent work describing these methods and difficulties can be found in Ref. [14]. The aim of this paper is to analyze the influence of a time-dependent external magnetic field on an anisotropic magnetic nanoparticle. In particular we study a periodic driving in the direction perpendicular to the main anisotropy direction (the easy axis) and a constant driving parallel to the easy axis.

Let us consider a magnetic particle and assume that it can be represented by a magnetic monodomain of magnetization $\mathbf{M}$, being governed by the dimensionless LLG equation

$$\kappa \frac{d\mathbf{m}}{d\tau} = -\mathbf{m} \times \mathbf{\Gamma} - \eta \mathbf{m} \times (\mathbf{m} \times \mathbf{\Gamma}), \tag{1}$$

where $\mathbf{m} = \mathbf{M}/M_s$, $\tau = t|\gamma|M_s$, and $\kappa = 1 + \eta^2$ [3,4]. Here M_s is the saturation magnetization that leads to $|\mathbf{m}| = 1$ and γ is the gyromagnetic factor, which is associated with the electron spin and whose numerical value is approximately given by $|\gamma| = |\gamma_e|\,\mu_0 \approx 2.21 \times 10^5\ \mathrm{m\,A^{-1}\,s^{-1}}$. In order to get better physical insight into the problem, let us evaluate the scales introduced here. Typical values are, e.g. for cobalt materials, $M_s \approx 1.42 \times 10^6$ A/m; hence the time scale ($\tau = 1$) is in the picosecond range, $t_s = 1/|\gamma|M_s \approx 3.2$ ps. The present technology is able to follow experiments at the femtosecond scale. Indeed, Beaurepaire *et al.* [15] observed the spin dynamics at a time scale below the picosecond scale in nickel [15]. More recently phenomena have been observed at a time scale less than 100 fs [16,17]. In Eq. (1), η denotes the dimensionless phenomenological damping coefficient that is characteristic of the material and whose typical value is of the order of 10^{-4}–10^{-3} in garnets and 10^{-2} or larger in cobalt or permalloy [3]. In Eq. (1) the effective magnetic field, denoted by $\mathbf{\Gamma}$, is given by $\mathbf{\Gamma} = \mathbf{h} + \beta\,(\mathbf{m} \cdot \hat{\mathbf{n}})\,\hat{\mathbf{n}}$, where $\mathbf{h} = \mathbf{H}/M_s$ is the external magnetic field and β measures the anisotropy along the $\mathbf{n}$ axis. This special type of anisotropy is called uniaxial anisotropy and the constant β can be positive or negative depending on the specific substance and sample shape [18] in use. We apply an external magnetic field $\mathbf{h}$ that comprises both a constant longitudinal and a

*laroze@mpip-mainz.mpg.de

periodic transverse part with fixed amplitude and frequency $\mathbf{h} = \mathbf{h}_0 + \mathbf{h}_T \sin(\Omega\tau)$, where $\mathbf{h}_0$ ($\|\hat{\mathbf{z}}$), $\mathbf{h}_T$ ($\perp\hat{\mathbf{z}}$), and Ω are time independent. We assume that the particle is fixed with the anisotropy axis along the constant field, $\mathbf{n} \| \hat{\mathbf{z}}$. We remark that $|\mathbf{m}|$ is conserved and Eq. (1) describes pure rotations of the magnetization in three-dimensional space. Many numerical schemes have been used to resolve the LLG equation [3] and to avoid numerical artifacts; it is suitable to solve Eq. (1) in the Cartesian representation [4].

For zero damping and without parametric forcing Eq. (1) is conservative. The dissipation and the oscillatory injection of energy drives the magnetic particle in an out-of-equilibrium situation. In such a circumstance the magnetization of the particle may exhibit complex dynamical behavior, e.g., quasiperiodicity, and chaos [4]. In Ref. [4] the existence of chaos as a function of $|\mathbf{h}_T|$ was discussed. In the following we provide a more exhaustive characterization of the chaotic regime including its dependence on the longitudinal field $|\mathbf{h}_0|$ and the frequency Ω, which will reveal a rather complicated topology in parameter space.

First, we characterize the dynamics of Eq. (1) by evaluating the Lyapunov exponents (LEs). This method consists in quantifying the divergence between two initially close trajectories of a vector field. In general, for a N-dimensional dynamical system described by a set of equations $dX^i/d\tau = F^i(\mathbf{X},\tau)$, the LEs are defined by

$$\lambda_i = \lim_{\tau\to\infty} \frac{1}{\tau} \ln\left(\frac{\|\delta X_\tau^i\|}{\|\delta X_0^i\|}\right), \tag{2}$$

where λ_i is the ith Lyapunov exponent and $\|\delta X_\zeta^i\|$ is the distance between the trajectories of the ith component of the vector field at time ζ. Let us recall that the measure of the exponential divergence in the phase space is given by the LEs and that one has as many LEs as one has dimensions of the phase space of the dynamical system [19].

Since our prototypical model conserves the modulus of the magnetization $|\mathbf{m}|$ and the applied magnetic field is time dependent, the effective dimension of the phase space is 3. Therefore, one could compute three LEs associated with the dynamics of Eq. (1). However, in terms of a dynamical system, only the largest LE (LLE) may become positive for a dissipative system of dimension 3. Here we explore the dependence of the LLE on the different control parameters of the system. One can, e.g., draw two-dimensional maps illustrating the magnitude of the LLE as a function of two parameters. This permits us to determine the parameter ranges that lead to chaotic dynamics, i.e., the LLE that is positive, and those showing regular (quasiperiodic, periodic, or fixed point) dynamics, i.e., the LLE that is zero or negative. In addition, following a technique explained in Ref. [14], we use an iterative zoom resolution process to investigate further the dependence of the dynamics upon very small variations of the system parameters.

In contrast, there are other methods of quantifying the nonperiodic behavior of a dynamical system such as the Fourier spectrum, Poincaré sections, and correlation functions [3,7,19]. Bifurcation diagrams using Poincaré sections of the dynamics of the magnetization angles, given by $\mathbf{m} = (\cos\phi \sin\theta, \sin\phi \sin\theta, \cos\theta)$, were employed in Ref. [4]. In these diagrams, when there is a continuum of points, the behavior is quasiperiodic or chaotic.

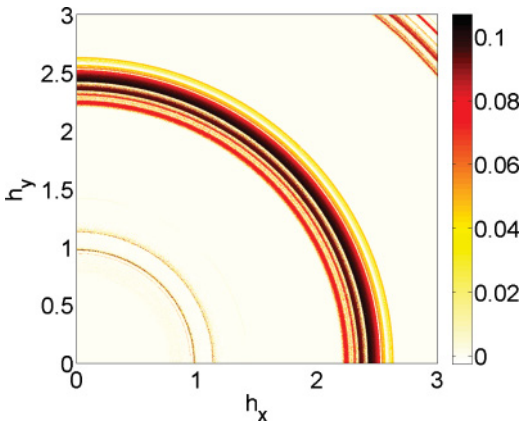

FIG. 1. (Color online) Phase diagram displaying the largest Lyapunov exponent color coded as a function of the field amplitudes h_x and h_y for $\Omega = 1$, $h_z = 0.1$, $\beta = 1$, and $\eta = 0.05$. The structure of the phase diagram is invariant with respect to the orientation of $\mathbf{H}_T$. The resolution is $\Delta h_x = \Delta h_y = 2\times10^{-3}$, namely, 1500×1500 discretization points.

We have integrated Eq. (1) in the Cartesian representation by using a standard fourth-order Runge-Kutta integration scheme with a fixed time step $d\tau = 0.01$ that ensures a precision of 10^{-8} on the magnetization field. The LEs are calculated for a time span of $\tau = 32768$ after an initial transient time of $\tau = 1024$ has been discarded. The Gram-Schmidt orthogonalization process is performed after every $\delta\tau = 1$. The error E in the evaluation of the LEs has been checked by using $E = \sigma(\lambda_M)/\max(\lambda_M)$, where $\sigma(\lambda_M)$ is the standard deviation of the maximum positive LE. In all cases studied here E is of the order of 1%, which is sufficiently small for the purpose of the present analysis. Due to the large number of parameters involved in the system, we set $\beta = 1$ and $\eta = 0.05$ for the rest of the paper.

Figure 1 shows a color-coded LLE phase diagram as a function of the oscillatory field amplitudes h_x and h_y. The chaotic regions appear in a circular symmetric fashion,

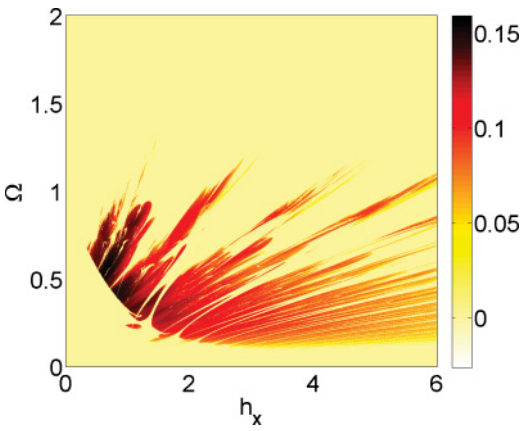

FIG. 2. (Color online) Phase diagram displaying the largest Lyapunov exponent color coded as a function of the field amplitude h_x and the frequency Ω for $h_y = 0$, $h_z = 0.1$, $\beta = 1$, and $\eta = 0.05$. The resolution is $\Delta\Omega = 2\times10^{-3}$ and $\Delta h_x = 3\times10^{-3}$.

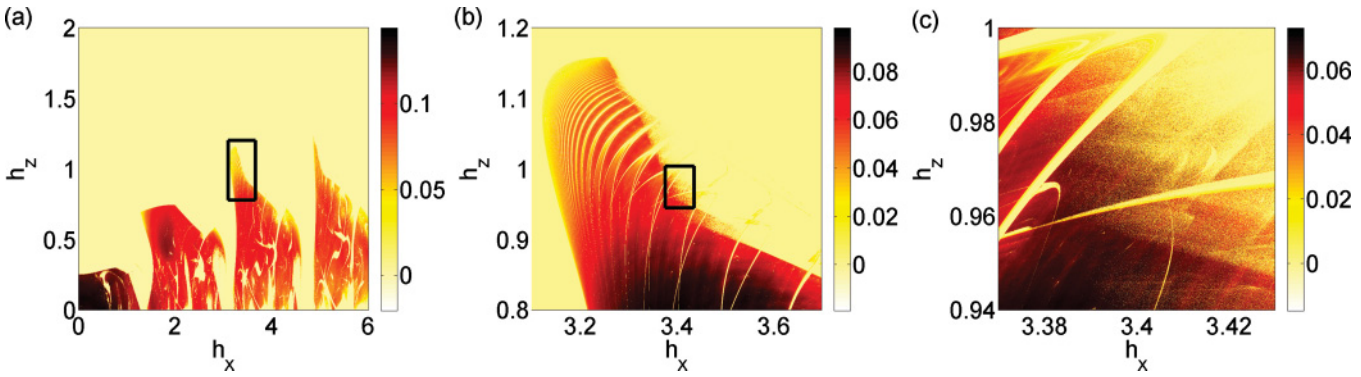

FIG. 3. (Color online) (a) Phase diagram showing a global view of the $h_x \times h_z$ space, computed for $\Omega = 0.5$, $h_y = 1$, $\beta = 1$, and $\eta = 0.05$. (b) Magnification of the black box in (a). (c) Magnification of the black box in (b). The parameter resolutions of these panels are (a) $\Delta h_x = 3\times10^{-3}$ and $\Delta h_z = 2\times10^{-3}$, (b) $\Delta h_x = \Delta h_z = 4\times10^{-4}$, and (c) $\Delta h_x = \Delta h_z = 4\times10^{-5}$.

indicating an invariance of the LEs with respect to the orientation of the periodic transverse field $\mathbf{h}_T$. For a general initial orientation of the magnetization, the full dynamical problem is not rotationally invariant. However, since the occurrence of chaos is independent of initial conditions and since there is only a single basin of attraction for the dynamics, the orientation of $\mathbf{h}_T$ in the perpendicular plane is irrelevant for the position of the regions with a positive LE. We observe that no chaos is found for small amplitudes of the oscillatory transverse field and that by increasing the field amplitudes, regions with chaos and those with regular dynamics alternate. In fact, the chaotic regions appear at almost constant intervals of $h_T = (h_x^2 + h_y^2)^{1/2}$.

Figure 2 shows the color-coded LLE as a function of the amplitude h_x and the frequency Ω of the time-dependent field at a small fixed value of the constant field h_z. For a given driving frequency, chaos occurs only above a certain field strength. Chaos appears first for a finite frequency, which corresponds roughly to the characteristic time scale of the magnetization dynamics. For smaller (and larger) frequencies the field has to be larger to experience chaos. Very small frequencies ($\Omega \lesssim 0.1$) and large frequencies ($\Omega \gtrsim 1.3$) hindered the appearance of chaos. Apparently, in both cases the time dependence of the driving force is instrumental for magnetization chaos because either the magnetization can follow it or it is averaged out. Interestingly, one can observe that inside the main chaotic areas there are still windows without chaos. For small fields and small frequencies the antagonistic nature of these two quantities for the appearance of chaos becomes clear, since chaos is only possible above a line $\Omega + h_x \approx$ const.

In Fig. 3 we investigate the dependence of chaos on the two amplitudes h_x and h_z of the periodic transverse and constant longitudinal fields, respectively. The ratio of these two amplitudes determines the angle of the periodic driving field with respect to the anisotropy axis. In Fig. 3(a) the global view for a rather large range of field values is displayed, while Figs. 3(b) and 3(c) show enlarged perspectives giving a more detailed picture. There is no chaos for a high constant field h_z, where its stabilizing effect dominates. For lower values of h_z, one observes again an alternation of chaotic and regular regions as one increases the h_x values. These alternating regions are reminiscent of the Arnol'd tongues that are observed in synchronization theory [20]. They look very similar to the reverberations present in damped-driven Duffing oscillators [21]. Note that the chaotic regions are not compact, but contain areas of regular dynamics for special values of the field amplitudes. The better resolution of Fig. 3(b), the zoomed-in

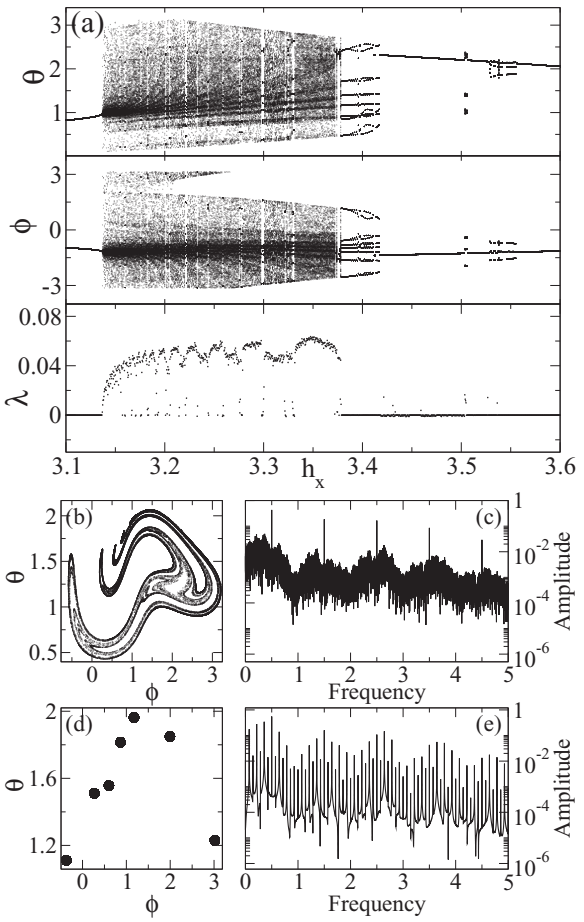

FIG. 4. (a) Bifurcation diagrams of θ and ϕ and LLE (λ) as a function of h_x. The fixed parameters are $\Omega = 0.5$, $h_y = 1$, $\beta = 1$, $\eta = 0.05$, and $h_z = 1$. Poincaré sections of ϕ and θ and the corresponding Fourier power spectra of m_x are shown for (b) and (c) $h_x = 3.35$ and (d) and (e) $h_x = 3.40$. The amplitudes of the power spectra are expressed in arbitrary units.

view of the white square seen in Fig. 3(a), reveals an interesting pattern in the form of a regular self-similar succession of chaotic and regular regions. Finally, by the next zooming step in the lowest frame [see Fig. 3(c)], one recognizes that the boundaries separating the chaotic and regular regions may be very complicated as they mix continuum branches with diffuse punctual separations.

Finally, in order to investigate in more detail different types of transitions between regular to chaotic behavior we analyze a horizontal cut of Fig. 3(b) in the range $3.1 \leqslant h_x \leqslant 3.6$ at $h_z = 1$. The bifurcation diagrams of θ and ϕ as a function of h_x are presented in Fig. 4(a). We observe that the system starts in a periodic state and makes an abrupt transition to a chaotic behavior. Above that, alternating regular and chaotic behaviors are found while increasing the parameter h_x. The middle and the lower parts of Fig. 4 show the Poincaré sections of ϕ and θ and the corresponding Fourier power spectra of m_x for two values of h_x, one in the chaotic [Fig. 4(b)] and the other in the regular regime [Fig. 4(d)], respectively. Figure 4(d) shows a Poincaré section consisting of seven isolated points, which describes a period-7 behavior.

In conclusion, we have determined the regions of parameters that lead to either chaotic or regular regimes using the Lyapunov exponent method. The azimuthal orientation of the transverse oscillating field is irrelevant here; however, the field strength, the angle of the applied field with respect to the easy axis, and the frequency of the forcing are crucial parameters for the appearance of chaos. For low frequencies and frequencies somewhat above the gyromagnetic resonance, no chaos is found, nor is it for weak transverse fields well below the saturation field strength. The static transverse field is stabilizing and suppresses chaos for higher field strengths. The parameter regions, where chaos does occur, are generally not compact, but consist of regular areas in an almost streaky fashion. Finally we mention that the complex structures of the several phase diagrams reported here are large enough to be experimentally accessible with present day technology and provide a means of testing the reliability of the underlying theoretical description.

D.L. acknowledges partial financial support from FONDECYT through Grant No. 11080229, Performance Agreement Project UTA/ Mineduc, and CEDENNA. Millennium Scientific Initiative through Grant No. P10-061-F. J.B. acknowledges financial support by MICINN through Grant No. FIS2008-06335-C02-02. J.A.C.G. was supported by CNPq, Brazil, and by USAFOSR.

[1] C. Ross, Annu. Rev. Mater. Res. **31**, 203 (2001).
[2] *Nonlinear Phenomena and Chaos in Magnetic Materials*, edited by P. E. Wigen (World Scientific, Singapore, 1994).
[3] I. D. Mayergoyz, G. Bertotti, and C. Serpico, *Nonlinear Magnetization Dynamics in Nanosystems* (Elsevier, Dordrecht, 2009), and references therein.
[4] L. F. Alvarez, O. Pla, and O. Chubykalo, Phys. Rev. B **61**, 11613 (2000).
[5] D. Laroze and P. Vargas, Physica B **372**, 332 (2006); D. Laroze and L. M. Perez, *ibid.* **403**, 473 (2008); D. Laroze, P. Vargas, C. Cortes, and G. Gutierrez, J. Magn. Magn. Mater. **320**, 1440 (2008); P. Diaz and D. Laroze, Int. J. Bif. Chaos **19**, 3485 (2009).
[6] D. V. Vagin and P. Polyakov, J. Appl. Phys **105**, 033914 (2009).
[7] R. K. Smith, M. Grabowski, and R. E. Camley, J. Magn. Magn. Mater. **322**, 2127 (2010).
[8] I. V. Barashenkov, M. M. Bogdan, and V. I. Korobov, Europhys. Lett. **15**, 113 (1991), and references therein.
[9] M. G. Clerc, S. Coulibaly, and D. Laroze, Phys. Rev. E **77**, 056209 (2008); Int. J. Bif. Chaos **19**, 2717 (2009); Physica D **239**, 72 (2010); Europhys. Lett. **90**, 38005 (2010).
[10] G. Gibson and C. Jeffries, Phys. Rev. A **29**, 811 (1984).
[11] F. M. de Aguiar, A. Azevedo, and S. M. Rezende, Phys. Rev. B **39**, 9448 (1989).
[12] J. Becker, F. Rodelsperger, Th. Weyrauch, H. Benner, W. Just, and A. Cenys, Phys. Rev. E **59**, 1622 (1999).
[13] J. Cai, Y. Kato, A. Ogawa, Y. Harada, M. Chiba, and T. Hirata, J. Phys. Soc. Jpn. **71**, 3087 (2002).
[14] J. A. C. Gallas, Int. J. Bif. Chaos **20**, 197 (2010), and references therein; J. G. Freire and J. A. C. Gallas, Phys. Rev. E **82**, 037202 (2010); Phys. Lett. A **375**, 1097 (2011); Phys. Chem. Chem. Phys. **13**, 12191 (2011).
[15] E. Beaurepaire, J. C. Merle, A. Daunois, and J. Y. Bigot, Phys. Rev. Lett. **76**, 4250 (1996).
[16] B. Koopmans, M. van Kampen, J. T. Kohlhepp, and W. J. M. de Jonge, Phys. Rev. Lett. **85**, 844 (2000).
[17] J. Hohlfeld, E. Matthias, R. Knorren, and K. H. Bennemann, Phys. Rev. Lett. **78**, 4861 (1997).
[18] R. C. O'Handley, *Modern Magnetic Materials: Principles and Applications* (Wiley Interscience, New York, 1999).
[19] H. Gould and J. Tobochnik, *An Introduction to Computer Simulation Methods: Applications to Physical Systems*, 2nd ed. (Addison-Wesley, New York, 1996).
[20] A. Pikovsky, M. Rosenblum, and J. Kurths, *Synchronization. A Universal Concept in Nonlinear Sciences* (Cambridge University Press, Cambridge, 2001).
[21] C. Bonatto, J. A. C. Gallas, and Y. Ueda, Phys. Rev. E **77**, 026217 (2008); A. R. Zeni and J. A. C. Gallas, Physica D **89**, 71 (1995); J. A. C. Gallas, Appl. Phys. B **60**, S203 (1995); C. Bonatto and J. A. C. Gallas, Phys. Rev. Lett. **101**, 054101 (2008); C. Bonatto, J. C. Garreau, and J. A. C. Gallas, *ibid.* **95**, 143905 (2005).